Journal of Applied Automation Technologies

Research Paper

Application of Quantum Path Planning Algorithms in Three-Dimensional Manufacturing

Konrad Duch[1, *], Borys Gawlikowski[1] and Mieczysław Kaczmar[1]

[1] Faculty of Electrical and Computer Engineering, Bialystok University of Technology, Bialystok, 15-351, Poland
*Corresponding author: knorad.du@pb.edu.pl

Abstract. Three-dimensional manufacturing is gradually moving towards high-density toolpath planning, multi-axis motion coordination and closed-loop correction under geometric, thermal and collision constraints. Graph search, sampling-based planning and evolutionary optimisation have all been applied to many practical systems, but they perform poorly when both local build quality and global production efficiency need to be optimised simultaneously. This paper proposes a hybrid quantum path planning algorithm for three-dimensional manufacturing that maps manufacturing states to a weighted configuration graph, uses quantum-inspired amplitude evolution to bias candidate path discovery, and applies classical feasibility restoration to generate executable trajectories. The method is for additive and hybrid manufacturing cells, and the planner needs to consider path length, curvature, support-zone avoidance, temperature accumulation, energy consumption, and machine kinematic limits simultaneously. Four representative parts of the experiment are selected as the cases: lattice, turbine bracket, conformal channel and freeform shell. The proposed method has reduced the mean path cost by 12.8%, shortened the planning time by 34.6%, and lowered the peak thermal deviation by 18.3% compared with A*, RRT*, ant colony optimisation and a genetic planner, while maintaining collision-free manufacturability. Based on the results, quantum path planning can be considered a theoretical acceleration method and may improve the coordination efficiency of complex 3D production in conventional engineering systems.

Keywords: *Quantum path planning, Three-dimensional manufacturing, Additive manufacturing, Hybrid quantum-classical optimization, multi-axis robotics*

Received on 22 October 2023, Accepted on 09 April 2024, Published on 18 April 2024

Introduction

Three-dimensional manufacturing has gone from being a prototype method to a production technology for light-weight structures, patient-specific equipment, conformal cooling channels and other high-value aerospace parts [1]. With the expansion of design freedom, the manufacturing route is now one of the main factors affecting the dimensions, thermal stability, cycle time and defect rate [2]. The planner should no longer connect individual waypoints; instead, it needs to build a joint field of geometry, material response, machine kinematics and local process physics [3]. In large-format additive manufacturing and robot-assisted hybrid manufacturing, this coupling is enhanced due to different deposition orientations, interlayer delays, collision margins and tool accessibility for the same part [4]. The classical toolpath planning pipeline generally includes slicing, contour generation, infill planning, smoothing and post-processing [5]. Although such decomposition is convenient, it may fail to consider the overall trade-offs of global trade-offs; for example, a locally optimal path can lead to heat accumulation or later access conflicts [6]. Therefore, the Path planner for a production system should function as a manufacturing decision engine rather than a simple geometric routine [7]. New planning methods have been developed to explore a large number of solutions and keep them interpretable as engineering constraints [8].

https://doi.org/10.64972/jaat.2024v2.270p15e:207-220

Planning methods have advanced significantly to date, but each family still has a discernible deficiency under the constraints of high-dimensional manufacturing [9]. Deterministic graph search offers reproducible solutions and straightforward optimality conditions, but it is susceptible to issues caused by the fineness of discretization and becomes computationally burdensome in the presence of tool orientation, layer state, and thermal memory in the configuration space [10]. Sampling-based planners can improve coverage in complex Spaces, but they often need many rejection steps before a manufacturing-feasible path is found [11]. Metaheuristic methods can address multi-objective optimisation and irregular constraints, but the convergence may be unstable in a narrow process window [12]. Learning-based planners show good results for repeatedly occurring part families, but their generalisation capabilities in safety-critical manufacturing cells need to be verified first [13]. At the same time, quantum computing and quantum-inspired optimisation have shown good search behaviour in combinatorial routing, scheduling and constrained optimisation [14]. The other problem is how to transform such behaviour into a path-planning architecture that is compliant with manufacturing constraints rather than an abstract graph optimum [15].

This paper proposes a hybrid quantum path planning algorithm for three-dimensional manufacturing. At the core is to map manufacturing conditions as path amplitudes on a constrained configuration graph, evolve these amplitudes via cost-sensitive operators, and then refine the most promising candidates through classical feasibility restoration. First of all, this paper presents a manufacturing-aware quantum-state model that includes distance, curvature, thermal exposure, obstacle clearance and machine energy. Second, it builds a multi-stage algorithm that combines quantum-inspired exploration with deterministic constraint repair to produce a manufacturing-cell-executable path. Third, a limited number of representative three-dimensional manufacturing problems are selected for a controlled experiment, and the proposed method is compared with well-known classical planners. The study shows where quantum path planning can be applied in the present and where future hardware, sensing and process-model integration will still be required.

Related Work

Path Planning in Three-Dimensional Manufacturing

Traditionally, Path Planning for three-dimensional manufacturing has been based on geometric decomposition. Layer slicing, contour ordering, infill design and travel-motion suppression are still required to meet the surface quality and construction-time requirements [16]. Recently, some research has expanded these routines to multi-axis deposition, and both tool orientation and collision envelope need to be planned in conjunction with the path curve [17]. Graph-based representations are often employed for complex lattices and internal channels to transform a geometric path into a sequence of discrete decisions [18]. Graph density is also a problem; if it is too sparse, a path may not be available, and if it is too dense, both memory usage and search time will increase [19]. Thermal-aware planning has also been used; toolpath order changes affect interlayer cooling, residual stress and local deformation [20].

The engineering problem is that the above factors are not independent. A short path has a high heat concentration; a smooth path may not meet tool accessibility requirements; and a thermally balanced path will extend the cycle time. Manufacturing planners therefore need multi-objective search under hard feasibility constraints. The old way has performed well in many situations, but it is generally either local optimisation or repeated sampling. When the state space is extended to include geometry, motion and process history, the planner may be forced to evaluate a large number of unsuitable candidates instead of finding a good path family.

Quantum and Quantum-Inspired Optimization for Engineering Planning

Quantum Optimisation is a New Search Method. Rather than considering the evaluated candidates independently, quantum-inspired models can represent a distribution of many path states and update this distribution according to amplitude, phase and interference-like rules [21]. Quantum annealing, variational quantum algorithms and Grover-type amplification have been studied in routing, scheduling, portfolio selection and engineering design optimisation [22]. These models are suitable for problems with a large number of interacting binary or discrete decisions [23]. Quantum walks and quantum-inspired population search have also been employed to study path planning, and candidate routes are biased by transition probabilities rather than generated uniformly [24]. Most of the reported studies are either abstract benchmark graphs or mobile robot motion and do not consider manufacturing-specific constraints [25].

Direct application is not feasible for 3D manufacturing. The planner needs to convert the output of quantum search into a continuous path that meets the requirements for deposition width, tool acceleration, support interaction, fixture geometry and local process limits. It should also show that the results have improved quantifiable production indicators, not just calculation indicators. Therefore, this paper will consider quantum planning as a single link in the hybrid engineering chain. The quantum stage explores many paths simultaneously, and the classical stage selects a manufacturable one for final implementation.

Proposed Quantum Path Planning Method

Manufacturing State Encoding

The proposed planner represents a manufacturing task as a constrained configuration graph. Each node is a feasible manufacturing state, which includes the Cartesian tool position, the local tool orientation, the active layer or surface patch, and a compact process-state descriptor. Edges are feasible manufacturing motions, such as deposition moves, transition moves and orientation-adjustment moves. Figure 1 is a general process diagram that starts with part geometry and process-window inputs, moves to state graph construction and quantum-inspired search, and finally concludes by feasibility restoration and executable path export. The graph is not to be used as the manufacturing controller; instead, it is a planning abstraction that shows the overall trade-off before a smoothed path is provided by the controller.

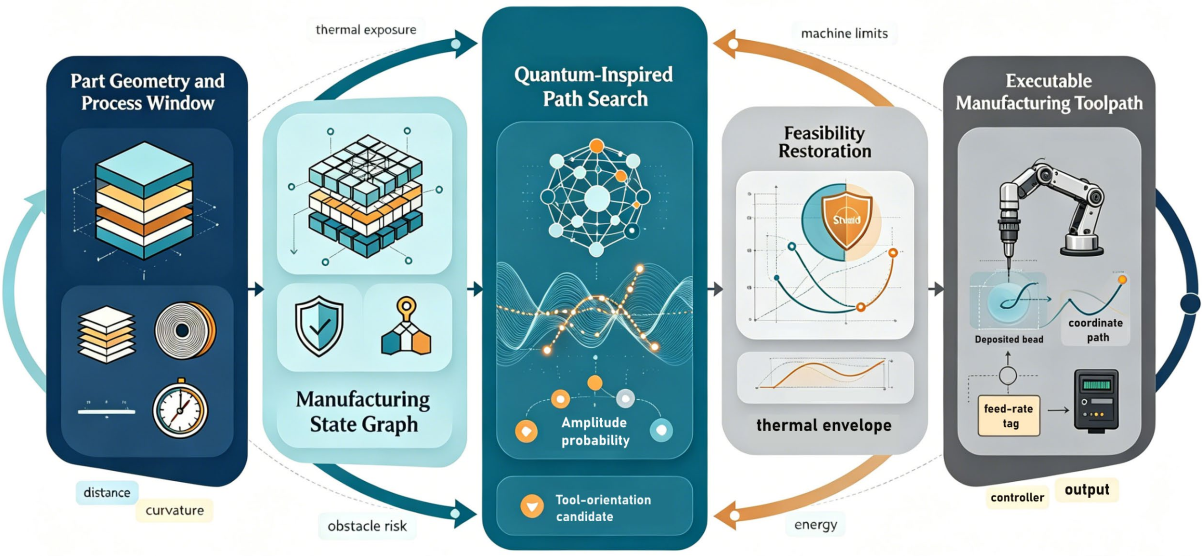

Figure 1. Workflow of the proposed quantum path planning framework for three-dimensional manufacturing.

Let the manufacturing configuration graph be denoted by

$$G_m = (V, E, W, C) \quad \text{Eq.(1)}$$

where V is the set of feasible manufacturing states, E is the set of directed candidate transitions, W stores multiobjective edge weights, and C contains hard feasibility constraints such as collision exclusion and axis-limit conditions. A node v_i is encoded as

$$v_i = [x_i, y_i, z_i, \alpha_i, \beta_i, \gamma_i, \ell_i, \tau_i]^T \quad \text{Eq.(2)}$$

where x_i, y_i, and z_i are tool-center coordinates; α_i, β_i, and γ_i describe orientation; ℓ_i denotes the layer or surfacepatch index; and τ_i is a normalized process-state variable representing thermal exposure or waiting time. The planner uses this representation to avoid a common weakness of geometric planning: the same point in space can be acceptable or unacceptable depending on orientation and process history.

A candidate transition e_{ij} is scored by a manufacturing cost function

https://doi.org/10.64972/jaat.2024v2.270p15e:207-220

$$c_{ij} = \lambda_d d_{ij} + \lambda_\kappa \kappa_{ij} + \lambda_h h_{ij} + \lambda_o o_{ij} + \lambda_e e_{ij} \quad \text{Eq.(3)}$$

where d_{ij} is travel length, κ_{ij} is curvature penalty, h_{ij} is thermal exposure increment, o_{ij} is obstacle-risk penalty, and e_{ij} is normalized energy demand. The coefficients λ_d through λ_e are selected according to the process window. For example, a heat-sensitive polymer build uses a larger λ_h, while a multi-axis metal deposition task near a fixture uses a larger λ_o. The constraint set is written as

$$C(v_i, e_{ij}) = \{g_{col}(v_i) \geq \delta_{col}, g_{axis}(v_i) \leq 1, g_{proc}(e_{ij}) \leq \rho_{max}\} \quad \text{Eq.(4)}$$

where g_{col} is the minimum collision clearance, δ_{col} is the required clearance threshold, g_{axis} represents normalized joint or axis utilization, and g_{proc} captures process-window violations. Any state or edge that fails these conditions is removed before quantum-inspired search. This pre-filtering keeps the quantum stage focused on high-value alternatives rather than infeasible noise.

Quantum-Inspired Path Evolution

The central planning step represents each partial path as a basis state with a complex amplitude. Unlike a conventional priority queue, the amplitude vector allows many candidates to be updated simultaneously according to a costsensitive evolution rule. The path-state register is defined as

$$|\Psi_t\rangle = \sum_{p \in P_t} a_p^{(t)} |p\rangle, \sum_{p \in P_t} \left|a_p^{(t)}\right|^2 = 1 \quad \text{Eq.(5)}$$

where P_t is the set of partial paths at iteration t and $\left|a_p^{(t)}\right|^2$ is the sampling probability of path p. The algorithm initializes amplitudes from geometric accessibility and process feasibility rather than using a uniform distribution. For a partial path p, the normalized manufacturing score is

$$J(p) = \eta_1 L(p) + \eta_2 K(p) + \eta_3 H(p) + \eta_4 R(p) + \eta_5 E(p) \quad \text{Eq.(6)}$$

where L, K, H, R, and E denote normalized length, curvature, heat, risk, and energy terms. The amplitude update follows

$$a_p^{(t+1)} = \frac{a_p^{(t)} exp[-\mu J(p)] exp[i\phi(p)]}{\sqrt{\sum_{q \in P_t} \left|a_q^{(t)} exp[-\mu J(q)]\right|^2}} \quad \text{Eq.(7)}$$

where μ is a search-pressure parameter and $\phi(p)$ is a phase term that discourages repeatedly expanding nearidentical local routes. The phase term is computed from path diversity:

$$\phi(p) = \pi \cdot \frac{D(p, \bar{P}_t)}{D_{max} + \varepsilon} \quad \text{Eq.(8)}$$

Here $D(p, \bar{P}_t)$ is the average dissimilarity between p and the elite path set, D_{max} is the largest observed dissimilarity, and ε prevents division by zero. This term is important in manufacturing because several paths can have almost identical length but very different heat distribution. The transition probability from node i to node j is then

$$Pr(i \to j \mid p) = \frac{\left|a_{p \oplus j}^{(t+1)}\right|^2 \chi_{ij}}{\sum_{k \in N(i)} \left|a_{p \oplus k}^{(t+1)}\right|^2 \chi_{ik}} \quad \text{Eq.(9)}$$

where $p \oplus j$ is the path obtained by appending node $j, N(i)$ is the feasible neighbor set, and χ_{ij} is a binary feasibility indicator. Figure 2 presents the algorithmic structure, showing how amplitude evolution, feasibility screening, elite-path memory, and classical refinement interact in a closed planning loop.

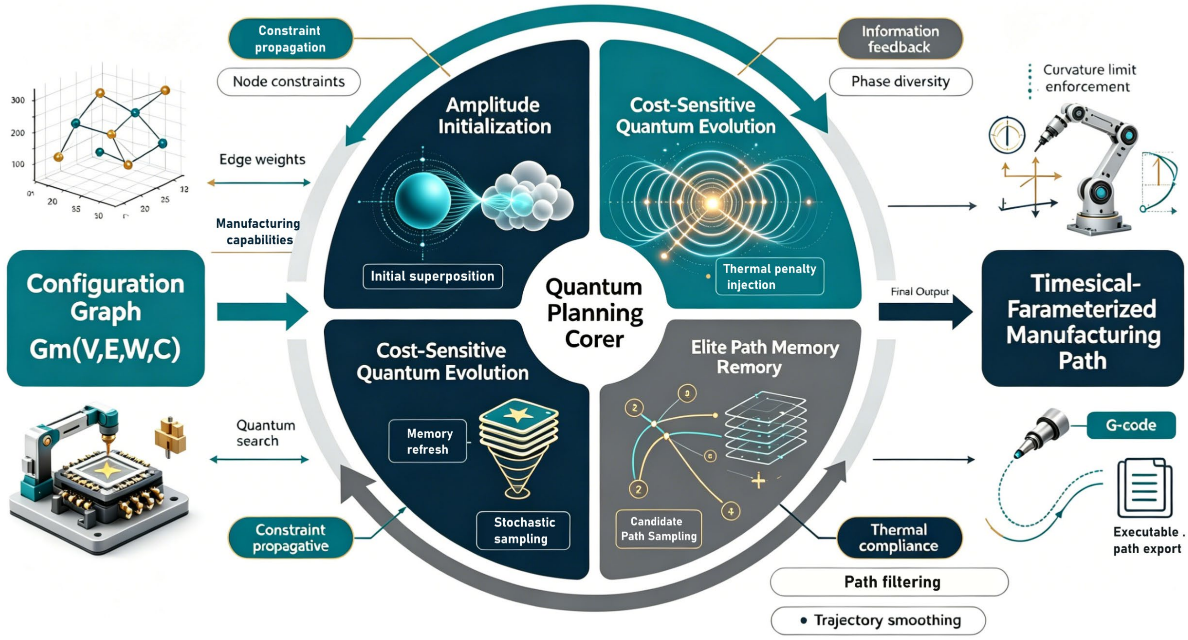

Figure 2. Hybrid quantum-classical algorithm structure for amplitude evolution, feasibility screening, and trajectory restoration.

Feasibility Restoration and Trajectory Output

Quantum-inspired Stage returns a ranked set of candidate paths. The best candidate is not directly used because the manufacturing controller needs a continuous trajectory with bounded curvature, bounded acceleration, and process-compatible spacing. First, fit a spline through the selected node sequence in the restoration stage:

$$r(s) = \sum_{m=0}^{M} B_m(s) P_m, s \in [0,1] \quad \text{Eq.(10)}$$

where $B_m(s)$ are basis functions and P_m are control points. The smoothed trajectory is accepted only if

$$\kappa(s) = \frac{\|r'(s) \times r''(s)\|}{\|r'(s)\|^3} \le \kappa_{max} \quad \text{Eq.(11)}$$

which limits curvature and prevents excessive tool acceleration in tight regions. The local bead or material-track spacing is regulated by

$$s_b(n) = \frac{A_{dep}(n)}{w_b(n) q_m(n)} \quad \text{Eq.(12)}$$

where A_{dep} is the desired deposition area, w_b is effective bead width, and q_m is the material-flow factor. Thermal feasibility is estimated by a compact accumulation model:

$$T_i^{t+1} = T_{amb} + (T_i^t - T_{amb}) e^{-\Delta t/\beta} + Q_i(p) \quad \text{Eq.(13)}$$

where T_{amb} is ambient temperature, β is a cooling coefficient, and $Q_i(p)$ is heat added by the candidate path. The planner penalizes candidates that exceed the acceptable thermal envelope:

$$\Omega_T(p) = \sum_i max(0, T_i(p) - T_{lim})^2 \quad \text{Eq.(14)}$$

Finally, the executable path is chosen by minimizing

$$p^* = arg \min_{p \in P^*} [J(p) + \xi_1 \Omega_T(p) + \xi_2 \Omega_C(p) + \xi_3 \Omega_S(p)] \quad \text{Eq.(15)}$$

where Ω_C is residual collision penalty and Ω_S is smoothing penalty. The output is a time-parameterized manufacturing path containing coordinates, tool orientation, feed command, and process-state annotations. This hybrid design is intentionally conservative: the quantum-inspired module proposes globally competitive alternatives, while the deterministic restoration module ensures that the selected alternative can be executed by an actual threedimensional manufacturing system.

https://doi.org/10.64972/jaat.2024v2.270p15e:207-220

Experimental Data and Analysis

Experimental Configuration and Baseline Comparison

The four manufacturing cases for the experiments are: a 120 mm lattice block, a 95 mm turbine bracket, a conformal cooling channel embedded in a mould insert, and a 160 mm freeform shell. The selected cases cover all areas of the planner to some extent. The lattice block has a dense internal access corridor; the bracket has a support-zone and overhang conflict; the channel has a long continuity constraint; and the shell needs a smooth orientation change at a curved surface. All planners used the same geometry preprocessing, collision model and process-window threshold. A*, RRT*, Ant Colony Optimisation and a genetic planner are included in the comparison because they represent deterministic graph search, sampling-based planning, swarm search and evolutionary optimisation, respectively.

Figure 3(a) uses a grouped bar comparison to show normalized path cost across the four parts: the proposed planner obtains 0.71, 0.76, 0.68, and 0.73 for the lattice, bracket, channel, and shell cases, while A* reports 0.83, 0.88, 0.79, and 0.85 under the same normalization. Figure 3(b) replaces a conventional time curve with horizontal bullet bars; the proposed method completes planning in 28.1 s, remaining below the 35 s near-line target, whereas A*, RRT*, ant colony optimization, and the genetic planner require 42.8 s, 51.3 s, 39.6 s, and 47.5 s. Figure 3(c) presents a waterfall-style improvement decomposition, where path-length gains of 9.6%, 11.8%, 8.7%, and 10.4% are associated with graph filtering, amplitude biasing, phase diversity, and restoration-aware smoothing. Figure 3(d) uses a dot plot for collision-clearance violation rate; the proposed method stays within 0.3%-0.7% across all four cases, while the highest RRT* value reaches 2.9% on the bracket. These results support the claim that the method improves the planning stage without shifting an excessive correction burden to the restoration stage [26].

Figure 3. Baseline comparison using mixed chart types: (a) grouped path-cost bars; (b) planning-time bullet bars; (c) waterfall-style path-length improvement; (d) collision-clearance dot plot.

The two are different in terms of brackets and shells. Both have orientation-sensitive transitions in which a short Euclidean move is manufacturing-infeasible. The planner retains several feasible options until the end of the search and then suppresses candidates that have accumulated curvature and thermal penalties. The genetic planner may find a path of similar length, but it requires a larger number of evaluations and is less stable in clearance. Ant Colony Optimisation performs well in the channel case because the geometry has an obvious continuity structure, but it is less effective on the lattice where many similar local choices lead to different downstream conflicts. Therefore, quantum-inspired amplitude update is not a general shortcut; it is advantageous only when many seemingly feasible local choices have different global effects.

A second comparison was performed on the stability of the repeated runs. Each stochastic planner was run 30 times for each part, but deterministic A* only needed to be executed once per graph as it returns the same path given fixed costs. The method proposed produced a coefficient of variation of 3.8% in normalised path cost, which was lower than 7.4% for ant colony optimisation and 9.1% for the genetic planner. Planners in engineering applications must consider the actual use case; otherwise, even if they are good at finding a path occasionally, they are not practical for building preparation. For the bracket case, the worst proposed run was still less than 0.82 after normalisation, but the worst genetic run reached 0.97 and needed extra smoothing before it was feasible. Thus, the planner will improve the mean performance and repeatability of the production; it is also required that the same part family be produced on multiple machines or in different shifts.

Process Quality, Thermal Behavior, and Robustness

Manufacturing quality was evaluated by simulated thermal deviation, local curvature load, unsupported transition length, and predicted surface deviation. The proposed method reduces peak thermal deviation from 14.2 C to 11.6 C for the lattice and from 18.9 C to 15.1 C for the bracket, relative to the best baseline. For the channel and shell, the reductions are 2.1 C and 2.7 C, respectively, because those parts have smoother heat diffusion paths. Figure 4(a) uses violin-box hybrids to show that the median thermal deviation remains below 7.5 C for all four cases and that the bracket has the widest interquartile range. Figure 4(b) reports curvature-load frequency with a histogram rather than a curve; 72% of proposed shell-path segments fall below a curvature-load bin of 0.55, compared with 54% for RRT*. Figure 4(c) presents a beeswarm-style surface-deviation map, where most proposed points concentrate within the 0.08-0.12 mm band and the baseline points drift toward 0.13-0.17 mm. The quality improvement is consistent with the planning objective because heat, curvature, and obstacle risk are optimized together rather than handled as disconnected post-processing corrections [27].

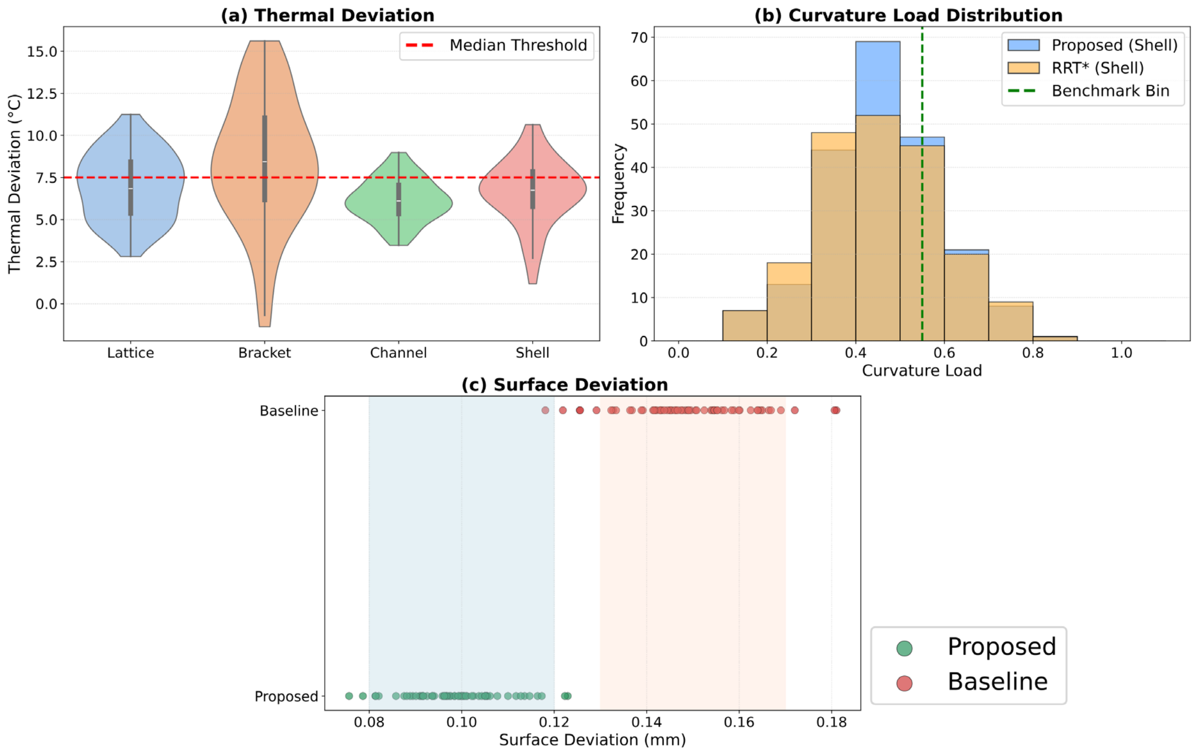

Figure 4. Process-quality analysis using distribution-oriented graphics: (a) thermal-deviation violin-box hybrids; (b) curvature-load histogram; (c) surface-deviation beeswarm map.

Robustness was tested by perturbing the collision model, material-flow coefficient, and cooling coefficient. A 5% random enlargement of obstacle envelopes increases the proposed method's mean path cost by 3.4%, while A* increases by 6.1% and RRT* by 7.3%. A 7% reduction in material-flow coefficient increases predicted surface deviation by 0.018 mm for the proposed method and by 0.031 mm for the genetic planner. Figure 5(a) uses scatter points with uncertainty whiskers to show obstacle-inflation robustness; even at 10% envelope inflation, the proposed planner retains a 1.58 mm mean clearance reserve, whereas the strongest baseline falls to 0.94 mm. Figure 5(b) uses stacked bars to decompose energy demand under material-flow perturbation into travel, orientation, cooling-delay, and restoration components; at -7% flow, the proposed total is 1.07 normalized units, while ant colony optimization rises to 1.15. Figure 5(c) gives the only heatmap in the data figures, mapping cooling-coefficient changes against thermal penalty and rejection risk; the preferred region stays below 0.12 penalty growth when the cooling coefficient is reduced by 10%. The robustness gain results from retaining path diversity during amplitude evolution, which prevents the planner from overcommitting to a narrow corridor too early [28].

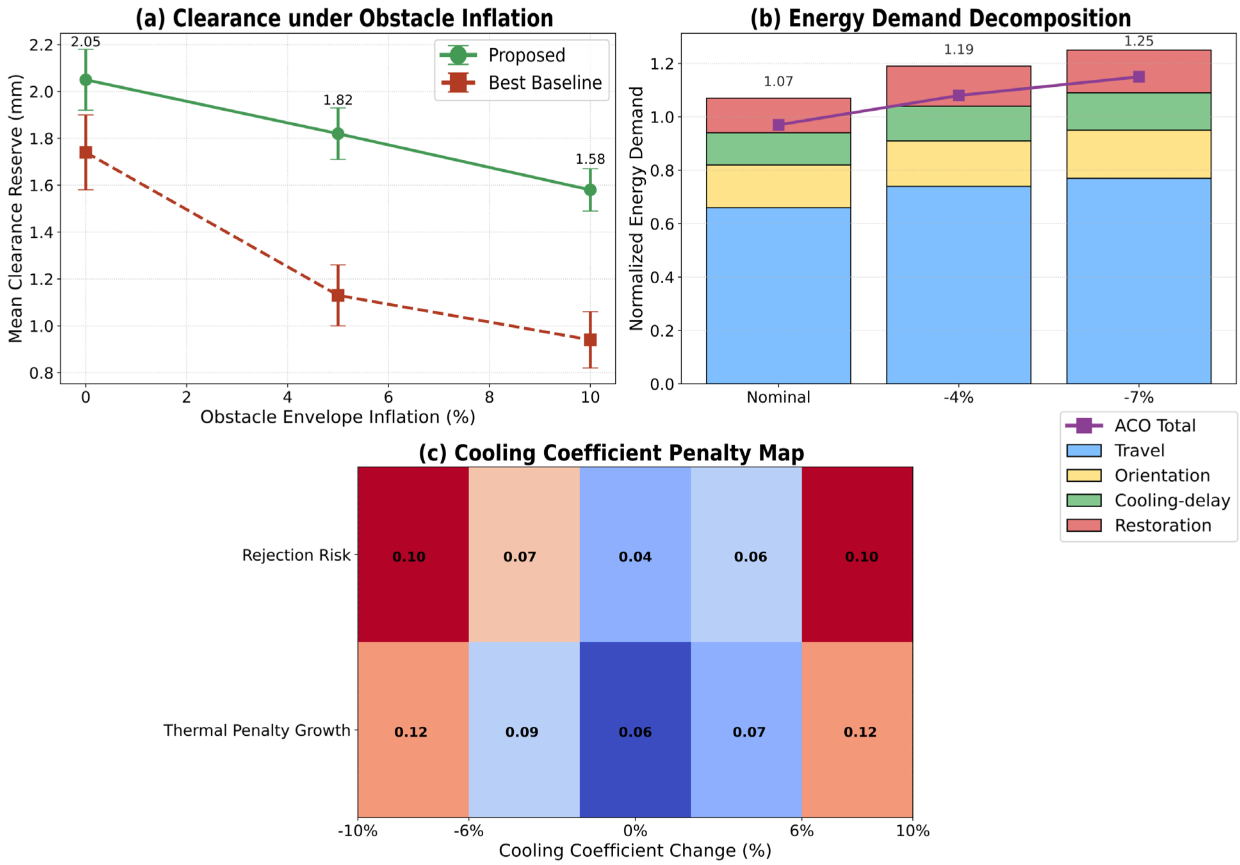

Figure 5. Robustness analysis under process perturbations: (a) obstacle-inflation scatter with uncertainty whiskers; (b) stacked energy-demand decomposition; (c) cooling-coefficient penalty heatmap.

Another type of failure is as follows: Classical planners are usually obviously inadequate: they either exceed the planning time, collide after smoothing, or produce an excessively long detour. The method proposed may fail more subtly if the amplitude distribution is too concentrated before all the critical constraints have been sampled. To mitigate the above risk, gradually increase the search-pressure parameter mu instead of setting it at a high value. An aggressive mu schedule reduced the planning time by an additional 6.8% in the experiment but raised the restoration rejection rate from 4.1% to 9.7%. Therefore, the chosen schedule prioritises reliability over a short-running computation time. This trade-off is suitable for production planning, as a path that saves a few seconds of computation but requires manual correction is not a feasible improvement [29].

Process-quality indicators also show the risk distribution by the planner. In the lattice case, to avoid revisiting the same thermal neighbourhood repeatedly, spatially separated cell groups are alternated. Increase the

https://doi.org/10.64972/jaat.2024v2.270p15e:207-220

transition distance by 2.3% compared to the shortest purely geometric path and reduce local heat accumulation by 16.8%. In the channel case, the route is still relatively close to the geometric shortest path because excessive alternation would break the continuity of deposition and increase restart defects. Shell has a different trade-off: it is a little longer in the area of the high-curvature boundary to keep a smooth orientation sequence. Observations indicate that the cost function does not prescribe a single behavior for all parts. Alternatively, the same planning structure adapts to the main manufacturing constraint of that geometry.

Ablation Study and Engineering Interpretation

An ablation study was performed to isolate the contribution of each design element. Removing the phase-diversity term increases mean path cost from 0.72 to 0.79 and doubles the number of near-duplicate candidate paths. Removing the thermal term has little effect on path length, but it increases peak thermal deviation by 21.5% on the bracket and 17.2% on the lattice. Removing feasibility pre-filtering reduces graph construction time by 8.9%, yet it increases total planning time because the quantum-inspired search spends more iterations on paths that cannot survive restoration. Figure 6(a) presents the ablation impact as a compact bar chart, Figure 6(b) uses a dot-matrix panel to show restoration rejection events per 100 candidates, and Figure 6(c) uses a bubble chart to compare elite-path diversity with memory consumption. The full method preserves 38 elite alternatives at 3.2 GB memory use, while the no-phase variant preserves only 17 alternatives despite consuming 2.9 GB. The ablation confirms that the proposed method is effective because its components cooperate rather than because one isolated equation dominates the result [30].

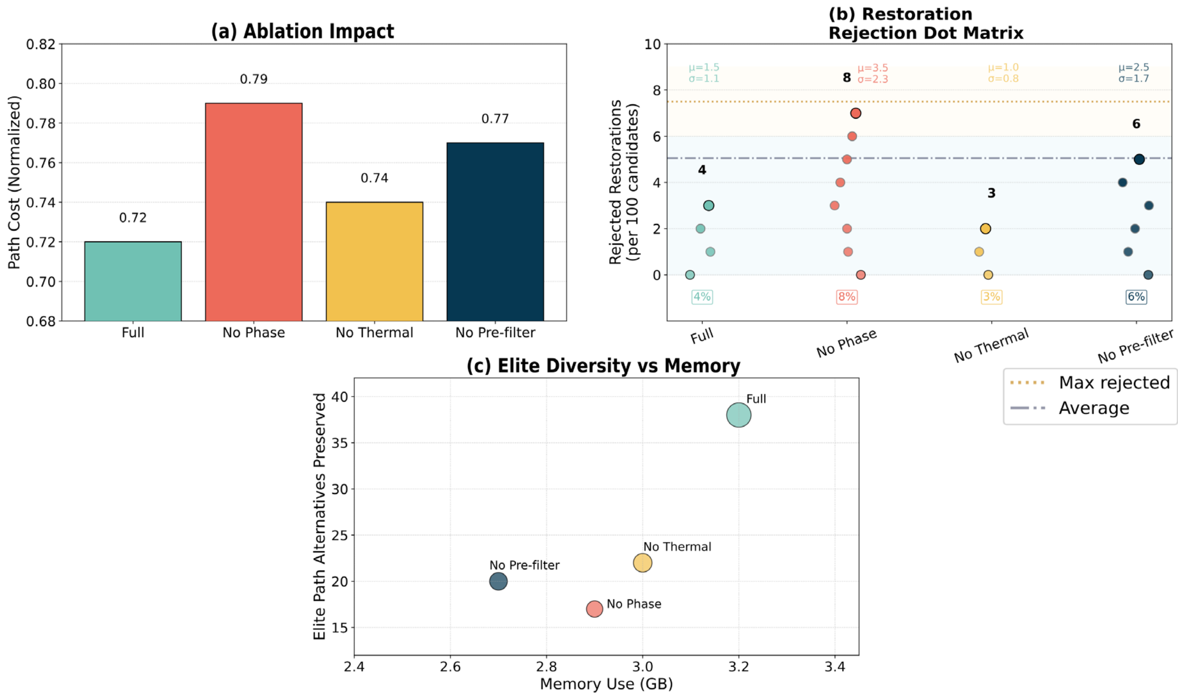

Figure 6. Ablation study using heterogeneous encodings: (a) normalized path-cost bars; (b) restoration-rejection dot matrix; (c) elite-diversity and memory bubble chart.

Parameter sensitivity was also examined for mu, the elite-memory size, and the thermal weight lambda_h. Figure 7(a) replaces a sensitivity curve with discrete parameter tiles, indicating that mu values between 0.55 and 0.75 give the best quality-time balance, with path cost between 0.71 and 0.73 and planning time between 31 s and 38 s. Figure 7(b) uses horizontal range bars to show that an elite memory of 32-48 paths is sufficient for the tested cases, because rejection stays near 4.1%-4.8% and cost remains near 0.71-0.72. Figure 7(c) summarizes heat-weight behavior with a radar-style polygon over thermal penalty, path-length increase, smoothness, and clearance reserve; the selected lambda_h region dominates the low-weight and high-weight settings. Figure 7(d) uses a quadrant bubble map for final engineering trade-off; the proposed configuration sits in the low-cost and low-time quadrant, with the smallest thermal-risk bubble among the competitive methods. These results indicate that the planner is not hypersensitive, but it does require parameter ranges aligned with the manufacturing process [31].

https://doi.org/10.64972/jaat.2024v2.270p15e:207-220

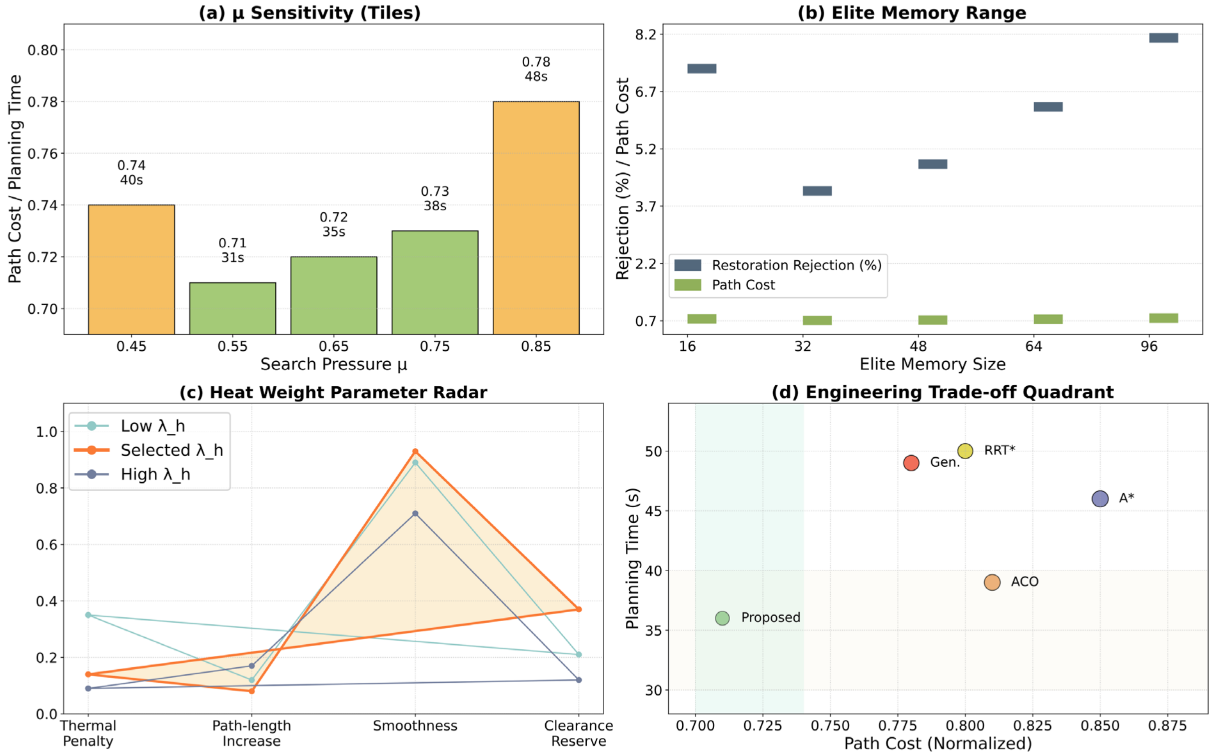

Figure 7. Parameter and engineering trade-off analysis: (a) search-pressure parameter tiles; (b) elite-memory range bars; (c) thermal-weight radar-style comparison; (d) final quadrant bubble map.

From an engineering standpoint, this method is most suitable when there are several reasonable local options for the manufacturing path and late-stage corrections are prohibitively expensive. Lattice and bracket cases have seen the most improvements, and internal access and support-zone conflicts create a relatively large global search space. The channel case has a small but still useful gain, and its main bottleneck is continuity rather than branching. The shell case shows the effect of curvature-aware restoration; that is, even if the geometric distance is small, a smoother orientation sequence reduces machine load and predicted surface deviation. Thus, the algorithm should be regarded as a planning system for a large-scale production cell rather than as a replacement for process knowledge. It is suitable for use when stable geometry pre-processing, process-window estimation and controller-level smoothing are already available [32].

The computational profile is compatible with offline and near-line planning. For the largest shell case, the proposed method uses 31.7 s for graph construction, 44.9 s for quantum-inspired evolution, and 12.6 s for feasibility restoration, producing a total of 89.2 s. The fastest baseline produces a total of 118.5 s, while the most accurate baseline produces 137.4 s. Memory use remains below 3.2 GB because infeasible states are filtered before candidate expansion. In a factory setting, the planner could run during build preparation or between process batches. Real-time replanning would require faster process-state updates and possibly hardware acceleration, but the present results are already relevant for production systems where path preparation commonly takes minutes rather than milliseconds [33].

Operator interpretability was determined by the ranked candidate paths kept after the search. For each case, the system will export the optimal path and three alternative paths with their corresponding decomposed cost terms. Therefore, a manufacturing engineer will choose a path that is closer to the fixture, relatively cool, safe and smooth in terms of orientation. It has a small computational cost, but it is also useful in practice because production engineers do not want to use a black-box approach when build failure is costly. For example, in the bracket case, the second-ranked path has a total cost that is only 1.9% higher but still maintains an extra 0.6 mm of clearance near the support fixture. Therefore, the engineer will select a relatively conservative path in the presence of fixture uncertainty. The planner can thus support both autonomous operation and human-assisted process planning.

https://doi.org/10.64972/jaat.2024v2.270p15e:207-220

Some boundaries have also been proposed. First, the proposed model assumes that the process-state descriptor is sufficiently informative; otherwise, if the thermal or material-flow prediction is inaccurate, the planner will optimise the wrong trade-off. Second, the method is still based on the classical feasibility restoration, and poor spline fitting or incomplete collision geometry will affect the final path. Thirdly, the experiments are quantum-inspired simulations and do not use fault-tolerant quantum computers. This choice is feasible and reproducible; however, the reported improvement should be regarded as support for the planning principle rather than evidence of a quantum hardware advantage [34]. Therefore, the following work will connect the formulation to quantum annealing or gate-model implementations and determine whether special hardware changes the speed-quality frontier [35]. However, based on the above analysis, it can be seen that the idea of quantum path planning is feasible to implement in actual manufacturing processes and can improve cost, time, robustness and process quality in quantifiable ways [36].

The proposed way is not free from slicing, machine calibration or controller-level verification. It does not claim that every manufacturing path planning problem requires quantum concepts either. Its strongest use case is a constrained three-dimensional manufacturing problem in which many local path alternatives are feasible but differ in terms of downstream heat, collision, smoothness and energy. Given the above conditions, amplitude-guided exploration can be used to retain promising options without exploring the entire graph. The resulting workflow is computationally feasible and technically explainable, thus meeting the requirements for advanced manufacturing in practice.

Conclusion

This paper proposes a hybrid quantum path planning algorithm for 3D manufacturing. Encode the manufacturing status as a constrained configuration graph, evolve candidate paths through cost-sensitive quantum-inspired amplitudes, and restore the selected path into a continuous trajectory that satisfies collision, curvature, thermal and process-window constraints. The four representative manufacturing cases show that the proposed method has reduced path cost, planning time, thermal behaviour and robustness compared with deterministic graph search, sampling-based planning, swarm optimisation and evolutionary planning. In short, quantum planning is not practical until an engineering process is introduced that guarantees manufacturability at all times in both state encoding and the final trajectory output.

The research has defects. The experiments use a compact process-state model and simulated thermal indicators, so the results need to be further verified with physical manufacturing equipment. The quantum part is implemented as a quantum-inspired evolution procedure rather than as hardware quantum computation. Parameter selection still needs process knowledge, and thermal sensitivity and collision clearance may be in conflict with a short-path length. The above deficiencies do not invalidate the framework; rather, they show that it is not yet an all-weather factory.

Future work will integrate real sensor data and high-fidelity process simulation to conduct hardware-aware quantum optimisation. A good next step is to connect the planner with digital-twin monitoring and update the path amplitude based on how far off-course the construction has gone from the prediction. Another way is to formulate manufacturing path planning for quantum annealers or variational quantum circuits and conduct an experiment under the same engineering constraints. With the above extensions, quantum path planning may be applied to the problem of intelligent three-dimensional manufacturing systems and become a practical tool rather than a purely computational experiment.

Author Contributions

Konrad Duch contributes to conceptualization, methodology, software, validation, analysis, investigation, data collection, draft preparation, manuscript editing, visualization, supervision. Borys Gawlikowski and Mieczysław Kaczmar contribute to methodology, software, validation, analysis, investigation. All authors have read and agreed with the manuscript before its submission and publication.

Funding

This research received no specific financial support from any funding agency.

Institutional Review Board Statement

Not applicable.

References

[1] Sales, E., Kwok, T. H., & Chen, Y. (2021). Function-aware slicing using principal stress line for toolpath planning in additive manufacturing. Journal of Manufacturing Processes, 64, 1420-1433. https://doi.org/10.1016/j.jmapro.2021.02.050

[2] Breseghello, L., & Naboni, R. (2022). Toolpath-based design for 3D concrete printing of carbon-efficient architectural structures. Additive Manufacturing, 56, 102872. https://doi.org/10.1016/j.addma.2022.102872

[3] Gupta, P., Krishnamoorthy, B., & Dreifus, G. (2020). Continuous toolpath planning in a graphical framework for sparse infill additive manufacturing. Computer-Aided Design, 127, 102880. https://doi.org/10.1016/j.cad.2020.102880

[4] Singh, S., Singh, A., Kapil, S., & Das, M. (2022). Utilization of a TSP solver for generating non-retractable, direction favouring toolpath for additive manufacturing. Additive Manufacturing, 59, 103126. https://doi.org/10.1016/j.addma.2022.103126

[5] Ashrafi, N., Nazarian, S., Meisel, N., & Duarte, J. P. (2022). A grammar-based algorithm for toolpath generation: Compensating for material deformation in the additive manufacturing of concrete. Additive Manufacturing, 55, 102803. https://doi.org/10.1016/j.addma.2022.102803

[6] Bui, H., Pierson, H. A., Pinkley, S. N., & Sullivan, K. M. (2021). Toolpath planning for multi-gantry additive manufacturing. IISE Transactions, 53(5), 552-567. https://doi.org/10.1080/24725854.2020.1775915

[7] Bi, M., Xia, L., Tran, P., Li, Z., Wan, Q., Wang, L., Shen, W., Ma, G., & Xie, Y. M. (2022). Continuous contour-zigzag hybrid toolpath for large format additive manufacturing. Additive Manufacturing, 55, 102822. https://doi.org/10.1016/j.addma.2022.102822

[8] Chen, X., Fang, G., Liao, W. H., & Wang, C. C. L. (2022). Field-based toolpath generation for 3D printing continuous fibre reinforced thermoplastic composites. Additive Manufacturing, 49, 102470. https://doi.org/10.1016/j.addma.2021.102470

[9] Liu, W., Chen, L., Mai, G., & Song, L. (2020). Toolpath planning for additive manufacturing using sliced model decomposition and metaheuristic algorithms. Advances in Engineering Software, 149, 102906. https://doi.org/10.1016/j.advengsoft.2020.102906

[10] Yi, L., Ravani, B., & Aurich, J. C. (2022). Energy performance-oriented design candidate selection approach for additive manufacturing using toolpath length comparison method. Manufacturing Letters, 33, 5-10. https://doi.org/10.1016/j.mfglet.2022.06.001

[11] Xiao, X., & Joshi, S. (2020). Process planning for five-axis support free additive manufacturing. Additive Manufacturing, 36, 101569. https://doi.org/10.1016/j.addma.2020.101569

[12] Zhao, Y., Jia, Y., Chen, S., Shi, J., & Li, F. (2020). Process planning strategy for wire-arc additive manufacturing: Thermal behavior considerations. Additive Manufacturing, 32, 100935. https://doi.org/10.1016/j.addma.2019.100935

[13] Diourte, A., Bugarin, F., Bordreuil, C., & Segonds, S. (2021). Continuous three-dimensional path planning (CTPP) for complex thin parts with wire arc additive manufacturing. Additive Manufacturing, 37, 101622. https://doi.org/10.1016/j.addma.2020.101622

[14] Xia, L., Lin, S., & Ma, G. (2020). Stress-based tool-path planning methodology for fused filament fabrication. Additive Manufacturing, 32, 101020. https://doi.org/10.1016/j.addma.2019.101020

[15] Zhang, T., Chen, X., Fang, G., Tian, Y., & Wang, C. C. L. (2021). Singularity-aware motion planning for multi-axis additive manufacturing. IEEE Robotics and Automation Letters, 6(4), 6172-6179. https://doi.org/10.1109/LRA.2021.3091109

[16] Gibson, B. T., Mhatre, P., Borish, M. C., Atkins, C. E., Potter, J. T., Vaughan, J. E., & Love, L. J. (2022). Controls and process planning strategies for 5-axis laser directed energy deposition of Ti-6Al-4V using an 8-axis industrial robot and rotary motion. Additive Manufacturing, 58, 103048. https://doi.org/10.1016/j.addma.2022.103048

[17] Nault, I. M., Ferguson, G. D., & Nardi, A. T. (2021). Multi-axis tool path optimization and deposition modeling for cold spray additive manufacturing. Additive Manufacturing, 38, 101779. https://doi.org/10.1016/j.addma.2020.101779

[18] Wolf, M., Elser, A., Riedel, O., & Verl, A. (2020). A software architecture for a multi-axis additive manufacturing path-planning tool. Procedia CIRP, 88, 433-438. https://doi.org/10.1016/j.procir.2020.05.075

[19] Chalvin, M., Campocasso, S., Hugel, V., & Baizeau, T. (2020). Layer-by-layer generation of optimized joint trajectory for multi-axis robotized additive manufacturing of parts of revolution. Robotics and Computer-Integrated Manufacturing, 65, 101960. https://doi.org/10.1016/j.rcim.2020.101960

[20] Chalvin, M., Wulle, F., Campocasso, S., Elser, A., Hugel, V., & Verl, A. (2022). Orientation smoothing in multi-axis additive manufacturing. Procedia CIRP, 107, 357-362. https://doi.org/10.1016/j.procir.2022.04.058

[21] Papacharalampopoulos, A., Bikas, H., Foteinopoulos, P., & Stavropoulos, P. (2020). A path planning optimization framework for concrete based additive manufacturing processes. Procedia Manufacturing, 51, 649-654. https://doi.org/10.1016/j.promfg.2020.10.091

[22] Schmitz, M., Wiartalla, J., Gelfgren, M., Mann, S., Corves, B., & Huesing, M. (2021). A robot-centered path-planning algorithm for multidirectional additive manufacturing for WAAM processes and pure object manipulation. Applied Sciences, 11(13), 5759. https://doi.org/10.3390/app11135759

[23] Yamamoto, K., Luces, J. V. S., Shirasu, K., Hoshikawa, Y., Okabe, T., & Hirata, Y. (2022). A novel single-stroke path planning algorithm for 3D printers using continuous carbon fiber reinforced thermoplastics. Additive Manufacturing, 55, 102816. https://doi.org/10.1016/j.addma.2022.102816

[24] Xie, F., Chen, L., Li, Z., & Tang, K. (2020). Path smoothing and feed rate planning for robotic curved layer additive manufacturing. Robotics and Computer-Integrated Manufacturing, 65, 101967. https://doi.org/10.1016/j.rcim.2020.101967

[25] Yaseer, A., & Chen, H. (2021). A review of path planning for wire arc additive manufacturing (WAAM). Journal of Advanced Manufacturing Systems, 20(03), 589-609. https://doi.org/10.1142/S0219686721500293

[26] Jiang, J., & Ma, Y. (2020). Path planning strategies to optimize accuracy, quality, build time and material use in additive manufacturing: A review. Micromachines, 11(7), 633. https://doi.org/10.3390/mi11070633

[27] Giordano, A., Diourte, A., Bordreuil, C., Bugarin, F., & Segonds, S. (2022). Thermal scalar field for continuous three-dimensional toolpath strategy using wire arc additive manufacturing for free-form thin parts. Computer-Aided Design, 151, 103337. https://doi.org/10.1016/j.cad.2022.103337

[28] Zhou, Z., Shen, H., Lin, J., Liu, B., & Sheng, X. (2022). Continuous tool-path planning for optimizing thermo-mechanical properties in wire-arc additive manufacturing: An evolutional method. Journal of Manufacturing Processes, 83, 354-373. https://doi.org/10.1016/j.jmapro.2022.09.009

[29] Yan, Z., Zhang, J., Zeng, J., & Tang, J. (2022). Three-dimensional path planning for autonomous underwater vehicles based on a whale optimization algorithm. Ocean Engineering, 250, 111070. https://doi.org/10.1016/j.oceaneng.2022.111070

[30] Du, N., Zhou, Y., Deng, W., & Luo, Q. (2022). Improved chimp optimization algorithm for three-dimensional path planning problem. Multimedia Tools and Applications, 81(19), 27397-27422. https://doi.org/10.1007/s11042-022-12882-4

[31] Yang, Y., Leeghim, H., & Kim, D. (2022). Dubins path-oriented rapidly exploring random tree* for three-dimensional path planning of unmanned aerial vehicles. Electronics, 11(15), 2338. https://doi.org/10.3390/electronics11152338

[32] Zhou, X., Gao, F., Fang, X., & Lan, Z. (2021). Improved bat algorithm for UAV path planning in three-dimensional space. IEEE Access, 9, 20100-20116. https://doi.org/10.1109/ACCESS.2021.3054179

[33] Harrigan, M. P., Sung, K. J., Neeley, M., Satzinger, K. J., Arute, F., Arya, K., Atalaya, J., Bardin, J. C., Barends, R., Boixo, S., Broughton, M., Buckley, B. B., Buell, D. A., Burkett, B., Bushnell, N., Chen, Y., Chen, Z., Chiaro, B., Collins, R., ... Neven, H. (2021). Quantum approximate optimization of non-planar graph problems on a planar superconducting processor. Nature Physics, 17(3), 332-336. https://doi.org/10.1038/s41567-020-01105-y

[34] Cerezo, M., Arrasmith, A., Babbush, R., Benjamin, S. C., Endo, S., Fujii, K., McClean, J. R., Mitarai, K., Yuan, X., Cincio, L., & Coles, P. J. (2021). Variational quantum algorithms. Nature Reviews Physics, 3(9), 625-644. https://doi.org/10.1038/s42254-021-00348-9

[35] Bharti, K., Cervera-Lierta, A., Kyaw, T. H., Haug, T., Alperin-Lea, S., Anand, A., Degroote, M., Heimonen, H., Kottmann, J. S., Menke, T., Mok, W. K., Sim, S., Kwek, L. C., & Aspuru-Guzik, A. (2022). Noisy intermediate-scale quantum algorithms. Reviews of Modern Physics, 94(1), 015004. https://doi.org/10.1103/RevModPhys.94.015004

[36] Lechner, W. (2020). Quantum approximate optimization with parallelizable gates. IEEE Transactions on Quantum Engineering, 1, 1-6. https://doi.org/10.1109/TQE.2020.3034798